3D FOREST STRUCTURE ESTIMATION FROM SAR TOMOGRAPHY BY MEANS OF A FULL RANK POLARIMETRIC INVERSION BASED ON COMPRESSIVE SENSING

Victor Cazcarra-Bes⁽¹⁾, Maria Tello-Alonso⁽¹⁾, Kostas Papathanassiou⁽¹⁾

(1)German Aerospace Center (DLR), P.O. Box 1116, 82234 Wessling, (Germany), Email: Victor.CazcarraBes@dlr.de, Maria.TelloAlonso@dlr.de, Kostas.Papathanassiou@dlr.de

ABSTRACT

SAR tomography (TomoSAR) techniques allow a direct 3D imaging by exploiting angular diversity with different passes of the sensor. One of the main drawbacks of SAR tomography is that the estimation of the vertical reflectivity profile has to be performed through a limited set of multibaseline acquisitions, which requires solving a highly underdetermined system of equations. In TomoSAR literature, the Capon and the Fourier beamforming spectral estimators are widely employed. As an alternative, the application of Compressive Sensing (CS) techniques to the estimation of forest profiles has been recently introduced. In this paper, a different algorithm based on CS is proposed. It performs a full rank polarimetric inversion, allowing thus an estimation of the 3D coherency matrices. To study the full rank polarimetric TomoSAR inversion, a temporal series of airborne data is used. The results of the 3D polarimetric inversion will be contrasted to in situ measurements and LIDAR data.

1. INTRODUCTION

SAR Tomography allows a 3D imaging of the forest body by exploiting angular diversity of a limited set of multibaseline acquisitions [1]. As shown in Fig.1, several passes of the sensor along the elevation axis are combined to estimate a 3D reflectivity of the illuminated area.

Considering the geometry represented in Fig.1 a stack of *M* SAR complex coherences is obtained. Each coherence can be expressed as:

$$y_m(x,r) = \int \beta(x,r,z) \exp(j k_T z) dz$$
 (1)

where x is the azimuth position, r is the slant range, y_m is the coherence obtained by the sensor, β is the radar reflectivity and k_z is the vertical wavenumber, which is a parameter that depends on the spatial baseline between the tracks orthogonal to the line of sight, the wavelength and the distance to the target. The cross-range resolution is determined by the largest distance between all the acquisitions (L_{tom}) while the non-ambiguous high interval is determined by the distance between two consecutive acquisitions (d).



Figure 1. Tomographic sensig operation using parallel passes

Eq. 1 shows that the vertical reflectivity profile at each slant range and azimuth positions can be derived from the stack of complex coherences, employing spectral estimation techniques. Since the number of acquisitions is limited, Eq. 1 is a highly underdetermined system. Currently, the most widely employed inversion techniques are the Capon and the Fourier beamforming spectral estimators, which can show a lower performance if the number of baselines is low and if they are not regularly distributed.

In order to solve the underdetermined linear problem in Eq.1, this paper presents an approach based on Compressive Sensing (CS) theory. Essentially, the theory of CS assumes that in a highly underdetermined system of equations, the unknown signal can be recovered from a few measurements with a high probability by solving a minimization problem, provided that it is sparse or compressible in a certain projection space and that the sensing matrix satisfies the Restricted Isometry Property (RIP) [2][3].

The remainder of this paper is organized as follows. In section 2 the formulation is presented. A rearrangement of the multibaseline covariance and the steering matrices is presented. The concept of sparsity is briefly introduced, the need of employing a sparsifying basis is deduced and the choice of a wavelet basis is justified.

Proc. 'PolInSAR 2015, Frascati, Italy 26–30 January 2015 (ESA SP-729, April 2015) Afterwards, experimental results are presented in Section 3. Conclusions and discussions are drawn in Section 4.

2. FULL RANK INVERSION BY MEANS OF CS

Taking M measurements over the same area, we can define for one polarization, a vector y which contains the reflectivity for each measurement as:

$$y_M = [y_1, y_2, \dots y_m]. \tag{2}$$

In case of having a fully polarimetric acquisition, for each track we get four different components HH, HV,VH and VV, that we can represent, for example as a Pauli basis. Therefore the vector of Eq.2 is transformed to a vector of 3M elements as:

$$y_{3M pauli} = [y_{HH+W_1}, y_{HH-W_1}, y_{2HV_1}, y_{HH+W_2}, \dots, y_{2HV_m}]$$
 (3)

This parameter is the complex reflectivity of the scene and it is a stochastic process. To characterize this process we need several realizations but as it is explained before, we are not able to take so many realizations. Nevertheless, assuming ergodicity we can make a multi-look in space to achieve more realizations.

To make this process, the second order statistics in the multibaseline covariance matrix is computed as:

$$[R]_{3Mx3M} = \langle y_{3M} \cdot y_{3M}^{H} \rangle = [\cdots] =$$

$$= \begin{bmatrix} \langle y_{HH+VV_1} \cdot y_{HH+VV_1} * \rangle & \dots & \langle y_{HH+VV_1} \cdot y_{2HV_m} * \rangle \\ \vdots & \ddots & \vdots \\ \langle y_{2HV_m} \cdot y_{HH+VV_1} * \rangle & \dots & \langle y_{2HV_m} \cdot y_{2HV_m} * \rangle \end{bmatrix}$$
(4)

where H denotes the hermitian vector and <> denotes a spatial multi-look.

Following Eq.1 the information related to the baseline and the position of the scatterer can be collected in the so called steering vector as:

$$\phi(z_0) = \begin{bmatrix} 1, \exp(jk_1z_0), \exp(jk_2 z_0), \dots \exp(jk_mz_0) \end{bmatrix}$$
 (5)

where z_0 is the vertical position. Therefore if we want to invert n-heights, the steering vector is converted to a steering matrix where the N heights combined with M measurements are represented.

Using the multibaseline covariance and the steering matrices, we can rewrite Eq. 1 as multiplication of matrices as follows [4][5]:

$$R_{CS} = \Phi_{CS} \cdot T \tag{6}$$

where ϕ_{cs} , is the steering matrix that it will define later in Eq.9, and T is a stack of coherency matrices along the height, which contains the estimated reflectivity for the desired heights from z = 0 to z = n defined as:

$$[T]_{Nx9} = \begin{bmatrix} T_{11} & T_{12} & \dots & T_{33} \\ T_{11} & z = 0 & & & z = 0 \\ T_{11} & & & & & \vdots \\ \vdots & & \vdots & \ddots & & \vdots \\ T_{11} & T_{12} & \dots & T_{33} \\ z = n & & & z = n \end{bmatrix}$$
(7)

where, for instance, T_{12} in z=0 is the coherency for channel HH+VV with HH-VV at the height z=0.

In order to be consistent with Eq. 6, the multibaseline covariance matrix (Eq. 4) is arranged in the following way:

$$\left[R_{cs} \right]_{M^{2}x9} = \begin{bmatrix} \left\langle y_{HH+VV_{1}} \cdot y_{HH+VV_{1}} \right.^{*} \left\rangle & \cdots & \left\langle y_{2HV_{1}} \cdot y_{2HV_{1}} \right.^{*} \right\rangle \\ \left\langle y_{HH+VV_{1}} \cdot y_{HH+VV_{2}} \right.^{*} \left\rangle & \vdots \\ \left\langle y_{HH+VV_{1}} \cdot y_{HH+VV_{m}} \right.^{*} \right\rangle & \cdots & \vdots \\ \left\langle y_{HH+VV_{2}} \cdot y_{HH+VV_{1}} \right.^{*} \left\rangle & \cdots & \left\langle y_{2H_{m}} \cdot y_{2HV_{m}} \right.^{*} \right\rangle \end{bmatrix} . (8)$$

Additionally, in the steering vector of Eq. 5, to form a matrix, the *n*-heights are included giving the following expression:

$$\left[\Phi_{cs} \right]_{M} 2_{xN} = \begin{bmatrix} e^{(jk_{0}z_{0})} \cdot e^{(-jk_{0}z_{0})} & \dots & e^{(jk_{0}z_{n})} \cdot e^{(-jk_{0}z_{n})} \\ e^{(jk_{0}z_{0})} \cdot e^{(-jk_{1}z_{0})} & & & & \\ e^{(jk_{0}z_{0})} \cdot e^{(-jk_{m}z_{0})} & & & & \\ e^{(jk_{0}z_{0})} \cdot e^{(-jk_{m}z_{0})} & & & & \\ e^{(jk_{1}z_{0})} \cdot e^{(-jk_{0}z_{0})} & & & & \\ e^{(jk_{m}z_{0})} \cdot e^{(-jk_{m}z_{0})} & & & & e^{(jk_{m}z_{n})} \cdot e^{(-jk_{m}z_{n})} \end{bmatrix} . (9)$$

As mentioned before, the CS theory is based in the idea of sparse signals; therefore to accomplish a good estimation, the signal should be sparse. A priori, we cannot assume that the signal is sparse, but we can project it in a sparsifying basis. [6].

As it is explored in [7][8] wavelet bases can be used to tackle the tomographic problem. Therefore, we can project the T matrix in a wavelet basis as:

$$W \cdot T = \alpha \tag{10}$$

where W is a matrix of N x N, which represents the wavelet transform and α are the sparse wavelet coefficients. From Eq.10 we can obtain the coherency matrix as follows:

$$T = W^{-1} \cdot \alpha \tag{11}$$

where W^{-1} denotes the inverse wavelet transform. Assuming an orthonormal wavelet W^{T} = W^{-1} .

The wavelet transform is defined by the mother wavelet employed and the number of scales or decomposition levels. Following the literature [9] in this paper we have chosen a Symmlet wavelet with 4 vanishing moments. Regarding the number of scales, we have empirically chosen 3 for the experimental part.

Combining Eq.6 and Eq. 11, we obtain the following expression:

$$R_{cs} = \Phi_{cs} \cdot W^{-1} \cdot \alpha \tag{12}$$

Eq. 12 represents an underdetermined problem with more unknowns than measurements (i.e with $\phi_{cs} \cdot W^I$ rectangular) that can be estimated using convex optimization, as:

$$\min \|T\|_{p, q} \quad s.t. \quad \begin{cases} R_{cs} = \Phi_{s} \cdot W^{-1} \cdot \alpha \\ T \text{ is semi - definite positive} \end{cases}$$
 (13)

where p,q is mixed norm. In this paper, in a first test a norm 2,1 has been used. For one side, we compute a L2 norm for the rows, indicating that different channels are not completely independent. On the other, the L1 norm for the columns looking for sparsity in the height dimension has been computed. In a second test, a norm $0,\infty$ enhancing the local maximum have been used.

Once we have the estimated wavelet coefficients of the optimization process, to retrieve the reflectivity we have to apply the inverse wavelet transform as follows:

$$\widetilde{\mathbf{T}} = \mathbf{W}^{-1} \cdot \widetilde{\boldsymbol{\alpha}} \tag{12}$$

where ~ denotes an estimation.

3. EXPERIMENTAL RESULTS

In order to study the Full rank PolTomoSar inversion, a dataset acquired in spring 2008 over the area of Traunstein, in the south-East of Germany, by the E-SAR system of the Microwave and Radar Institute of the DLR is used. The data is fully polarimetric acquired at L-band using 5 non-uniform baselines from 5 to 25 meters. The area under study is constituted by a highly heterogeneous managed forest (the highest height around 25 ~ 35 meters) in a temperate climate, with coniferous, deciduous and mixed stands at different growth stages. In Fig.2 the amplitude of SLC for HH channel is shown.

The SLC resolution is 2.12 m in range and 1.2 m in azimuth. Taking this into account we choose a spatial multilook of 5x11 applying a boxcar filter with an overlap window of 2 pixels in range and 5 pixels in azimuth.

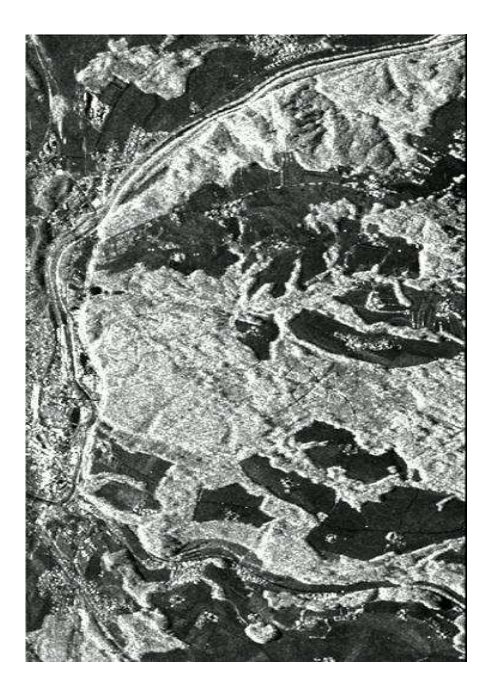


Figure 2. SLC SARAmplitude image of the test side in Traunstein, Germany.

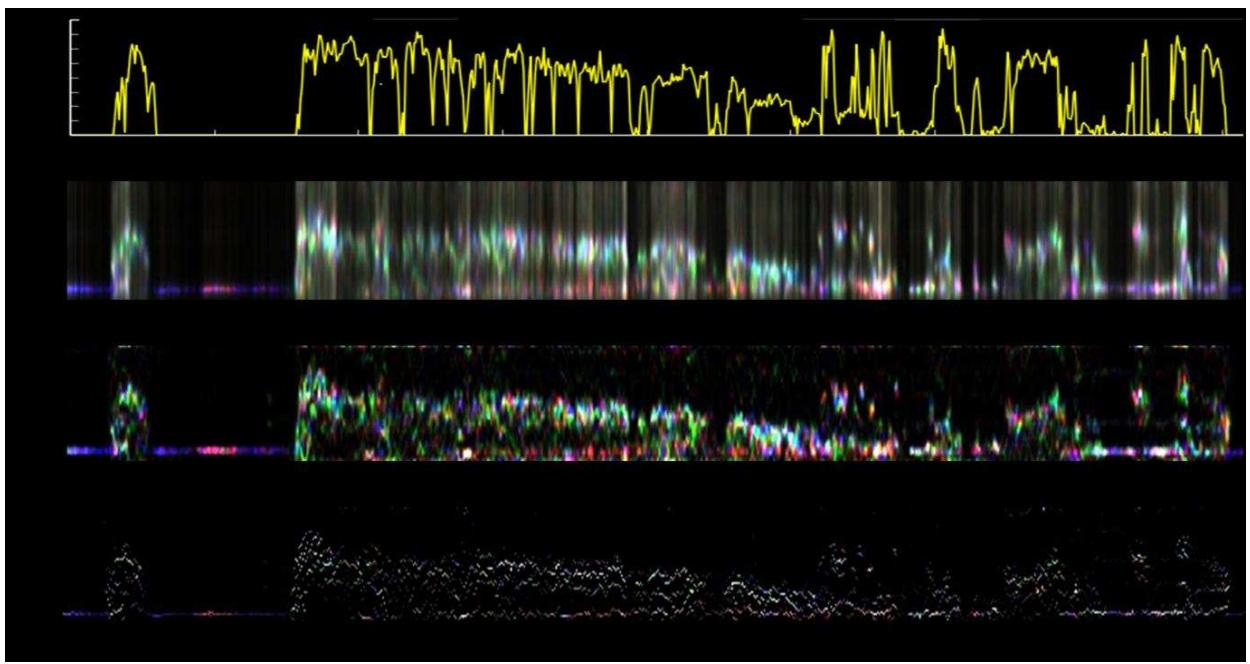


Figure 3. Tomograms in azimuth direction (850 pixels). Reference Lidar data (a), pauli representation HH+VV in blue, HH-VV in red and HV+VH in green for capon beam forming (b), using CS with norm 2,1 (c) and using CS with norm $0,\infty$ (d)

As auxiliary data, a LIDAR measurements are available over the same area. Moreover, a data in a known position, called also inventory plot, have been used. The data collected in a single inventory plot is composed by the number, height and position of the trees in a radius of 12.5 meters.

As it has been explained before, Eq. 11 represents a convex optimization problem. Two options have been tested: The CVX Matlab interface with the SDPT3 solver [10] and the Spams toolbox using the python interface [11].

3.1. Full rank tomograms

In Fig.3 the results obtained for a range slice are shown. The Fig.3a shows the LIDAR height of the same area, while in Fig. 3b, Fig. 3c and Fig. 3d the Pauli tomograms for 850 pixels in azimuth using the capon inversion are shown.

Related to CS results in Fig.3c the norm 2,1 and in Fig. 3d the nom $0,\infty$ are shown. Comparing the CS results with the lidar measurement presented in Fig.3a, it is possible to observe that the CS result is less affected by side-lobes.

Analysing the polarimetric information of CS profiles, as we expected in the parts where there is only ground, we obtain single bounce (blue colour) while in the canopy the volume scattering (green) is predominant. Moreover, in some parts of the ground we also observe a green colour, which might be a contribution coming

from the double bounce in the canopy layer that appear in the ground.

Comparing now the Fig. 3c with Fig. 3d, it seems that we can distinguish better the different layers (ground and canopy) in the later.

3.2. Inventory plots

In this part of the results, the global idea is to take the inventory plots and use them as a reference. In a first step with LIDAR and after with the estimated reflectivity using the CS inversion.

For validation purposes, during the study different kind of inventory plots have been used. To summarize the idea and the conclusions obtained with inventory plots, two examples have been included in this paper. For the first example, in Fig. 4, the representation of the inventory plot is shown. In that specific example, the inventory plot is composed by one layer of canopy of the same tree species. As a first comparation, in Fig. 4b the representation of LIDAR is shown. In this figure, each point represents a return and the colour code corresponds to height, red means high points and blue low points. Also, in Fig. 4c the power of reflectivity obtained by the CS inversion is shown. In that case, the width of the point indicates the power (wider means more power), and the colour represents again the height.

As a second example, a different inventory plot composed by one tall tree and a small canopy layer with two species is shown in Fig. 5. It is important to take into account that there are sources of error and uncertainty. The geo-location for the inventory plots in the LIDAR and radar data can have some errors and of course this could affect the interpretation of the results using a small area with a radius of 12.5 meters for validation.

Starting with the first example, in the results obtained, a clear similitude between LIDAR and Radar in the global structure is appreciated. In both cases the amount of trees are located in the left part of the figure, while in the right part only a few contribution, may be due to a single tree, is represented. With respect to the layer structure, in the radar example we can distinguish the two layers (ground and volume) that the inventory plot indicates

Regarding to the second example, in this case again there is a similarity between the inventory and the 3D representation of radar and LIDAR. The position and the reflectivity of the single tree are represented. Moreover, as it is shown in Fig.5c the lower layer can be distinguished.

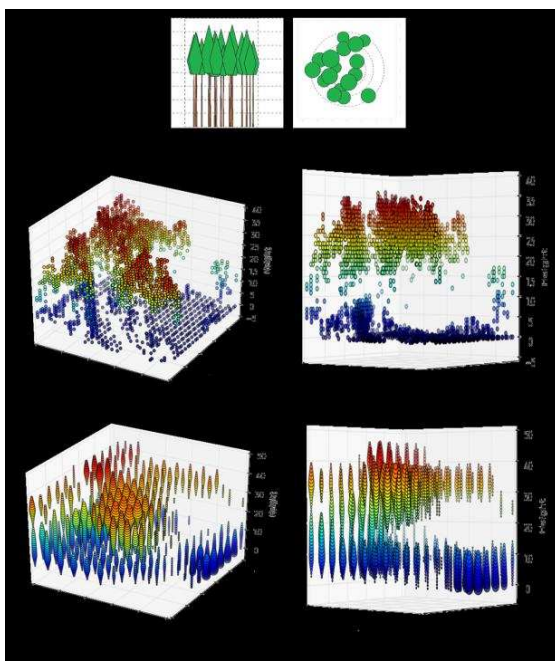


Figure 4. Example 1 of inventory plot data (a.1 and a.2), Lidar data (b.1 and b.2) and power obtained using CS with norm 2,1 (c.1 and c.2)

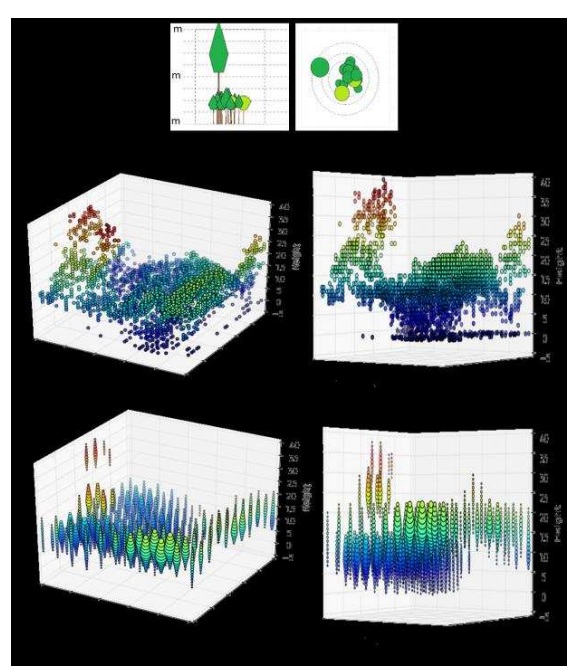


Figure 5 Example 2 of inventory plot data (a.1 and a.2), Lidar data (b.1 and b.2) and power obtained using CS with norm 2,1 (c.1 and c.2)

4. CONCLUSIONS AND DISCUSSION

In this paper, a full rank polarimetric inversion using CS has been presented, in order to estimate the 3D forest structure. As it has been exposed in section 2, the manipulation of the steering and covariance matrices in combination with the wavelet transformation, allows us to define the tomographic problem as a convex optimization problem.

In the first analysis using Pauli representation, we found out a correspondence between the 3D structure observed in the inventory data, in the LIDAR and in the estimated radar backscattering using CS.

The future work and studies will focus in a first step on the optimization and the further analysis of the CS implementation. The analysis of different norm to get different results, the study of the wavelet transformation to achieve a better performance and also the use of conditioned matrix to increase the goodness of the estimation process. As a second step, the idea is to extend the analysis to understand forest structure change signatures (dynamics due to weather, seasonal and/or disturbance and regrowth effects). Furthermore, the analysis of polarimetric information in order to retrieve physical information of the forest will be done.

5. REFERENCES

- [1] A. Reigber and A. Moreira. "First demonstration of airborne SAR tomography using multibaseline L-band data". IEEE Trans. Geosci. Remote Sens., Vol. 38, No. 5, pp. 2142–4152, Sep. 2000.
- [2] E. Candes and M. Wakin, "An Introduction To Compressive Sampling" IEEE Signal Processing Magazine, vol. 25, no. 2, pp. 21–30, Mar. 2008.
- [3] R. Baraniuk. "Compressive Sensing". IEEE Signal Processing Magazine, 24(4), pp. 118-121, 2007.
- [4] E. Aguilera, M. Nannini, and A. Reigber. "A data-adaptive compressed sensing approach to polarimetric SAR tomography of forested areas". IEEE Geosci. Remote Sens. Lett., Vol. 10, No. 3, pp. 543–547, May 2013.
- [5] E. Aguilera, M. Nannini, and A. Reigber. "Multisignal compressed sensing for polarimetric SAR tomography". IEEE Geosci. Remote Sens. Lett., Vol. 9, No. 5, pp. 871–875, Sep. 2012.
- [6] E. Aguilera, M. Nannini, and A. Reigber. "Wavelet-based compressed sensing for SAR tomography of forested areas". IEEE Trans. Geosci. Re- mote Sens., Vol. 51, No. 12, pp. 5283–5295, Dec. 2013.
- [7] S. Bhattacharya, T. Blumensath, B. Mulgrew, and M. Davies. "Synthetic aperture radar raw data encoding using compressed sensing". In: Radar Conference, 2008. RADAR '08. IEEE, pp. 1–5, May. 2008
- [8] L. Potter, E. Ertin, J. Parker, and M. C, etin. "Sparsity and compressed sensing in radar imaging". Proceedings of the IEEE, Vol. 98, No. 6, pp. 1006–1020, Jun. 2010.
- [9] S. Mallat. A wavelet tour of signal processing. Academic Press, Burlington, 2009
- [10] M. Grant and S. Boyd, CVX: Matlab Software for Disciplined Convex Programming. [Online]. Available: http://cvxr.com/cvx
- [11] SPAMS (SPArse Modeling Software) optimization toolbox for solving various sparse estimation problems. [Online]. Available: http://spams-devel.gforge.inria.fr/
- [12] L. Ferro-Famil, Y. Huang, and A. Reigber. High-resolution SAR tomography using full rank polarimetric spectral estimators. Proc. IGARSS, July 2012.